

# Absorbed photodynamic dose from pulsed versus continuous wave light examined with tissue-simulating dosimeters

Brian W. Pogue, Lothar Lilge, Michael S. Patterson, Brian C. Wilson, and Tayyaba Hasan

A dosimetric system has been developed to measure the spatially resolved light dose absorbed by a photosensitizer in a tissue-simulating medium. These gelatin-based dosimeters had macroscopic optical scattering and absorption properties that are typical for homogeneous tissue and contained the photosensitizer benzoporphyrin derivative monoacid (BPD-MA). A reporter molecule, 2',7'-dichlorofluorescein diacetate (DCF-DA), served as an actinometer, which could be photosensitized by BPD-MA to generate a highly fluorescent photoproduct. The relative photosensitizing efficiencies of high-intensity pulsed and cw laser light were compared in these tissue-simulating dosimeters. These measurements demonstrate an increase in penetration for pulsed light as compared with cw light in the dosimeters. A numerical simulation of the light propagation based on optical diffusion theory was used along with the energy levels of the photosensitizer molecule to examine the mechanisms involved in the absorbed dose. The increased penetration of high-intensity pulsed light was due to a transient decrease in the absorption of the photosensitizer, resulting from saturation of the photosensitizer optical transitions. This study provides the first direct comparison of the photodynamic dose absorbed by a photosensitizer using both high-intensity pulsed and cw laser light in a tissue-simulating medium. These measurements demonstrate that a small increase in depth of treatment is possible with pulsed laser light as compared with cw laser light simply on the basis of the unique photochemistry of the photosensitizer. However, this effect still needs to be examined carefully in tumor tissue, where other biological or chemical effects may become significant. © 1997 Optical Society of America

*Key words:* Photodynamic therapy, photosensitizer, benzoporphyrin derivative, tissue optical property, tissue phantom.

## 1. Introduction

Photodynamic therapy (PDT) is an experimental treatment, primarily for solid tumors, involving the systemic or local administration of a photosensitizing

drug, which is somewhat preferentially accumulated in neoplastic tissues.<sup>1,2</sup> The diseased tissue is then irradiated with light of the appropriate wavelength to cause electronic excitation of the drug, leading ultimately to tumor necrosis through a cascade of photochemical reactions. The mechanisms of cell death are currently being studied by many researchers<sup>3-5</sup> and clinical trials using various photosensitizers are in progress for a variety of diseases.<sup>1,6-8</sup> Approval from regulatory authorities has been obtained internationally for the treatment of selected cancers with Photofrin (QLT Phototherapeutics Inc., Vancouver, Canada), and this therapy has recently been approved by the U.S. Food and Drug Administration for treatment of advanced-stage esophageal cancer. These approvals are likely to lead to more common use of this treatment modality.

One of the major limitations of PDT is the limited penetration of light in tissue, permitting effective treatment depths of only several millimeters, de-

---

When this research was done, B. W. Pogue and T. Hasan were with the Department of Dermatology, Wellman Laboratories of Photomedicine, Harvard Medical School, Massachusetts General Hospital, Boston, Massachusetts 02114. B. W. Pogue is now with the Thayer School of Engineering, Dartmouth College, Hanover, New Hampshire 03755 (Brian.Pogue@Dartmouth.edu). L. Lilge and B. C. Wilson are with the Ontario Cancer Institute, Princess Margaret Hospital, Toronto, Ontario M5G 2M9, Canada. M. S. Patterson is with the Hamilton Regional Cancer Centre and McMaster University, Hamilton, Ontario L8V 5C2, Canada. Reprint requests should be addressed to T. Hasan.

Received 17 June 1996; revised manuscript received 28 October 1996.

0003-6935/97/287257-13\$10.00/0

© 1997 Optical Society of America

pending on the wavelength used.<sup>9,10</sup> Since red and near-infrared light has the lowest absorption in most tissues,<sup>11</sup> many recent studies have focused on finding second generation photosensitizers with strong absorption bands in the 600–800 nm range<sup>12</sup> to allow higher penetration while maintaining high absorption by the photosensitizer. However, high absorption by the photosensitizer in tissue can actually limit the penetration of the excitation light, lowering the effective treatment depth by decreasing the light transmitted to deeper tissues. This prediction has been confirmed experimentally in normal rat liver.<sup>13,14</sup>

The photosensitization process is generally thought to result from quenching of excited triplet-state photosensitizer molecules by molecular oxygen to produce reactive singlet-state molecular oxygen. Most sensitizer molecules have singlet-state lifetimes in the nanosecond range and triplet-state lifetimes in the microsecond range in aqueous media.<sup>15</sup> Excitation of the photosensitizer with high-intensity laser pulses can cause a depletion of the ground state, which would cause a transient change in the photosensitizer absorption. Thus the leading edge of a nanosecond laser pulse can excite most of the photosensitizer in the surface tissue layers, and produce a lower attenuation for the rest of the pulse traveling through the same tissue. Okunaka *et al.*<sup>16</sup> examined the average depth of tumor necrosis from PDT with hematoporphyrin derivative in a mouse kidney tumor model and observed an increase from 4 mm with cw excitation to 15 mm with 11-ns pulsed irradiation for a fixed radiant exposure of 50 J/cm<sup>2</sup>. Recent modeling by Patterson and Wilson<sup>17</sup> predicted increases in the light penetration from pulsed laser irradiation with second generation photosensitizers, where the ground-state absorption of the sensitizer was appreciable at the excitation wavelength.

Pulsed irradiation has also been investigated recently as a method of achieving oxygen-independent photosensitization. Andreoni<sup>18</sup> first demonstrated that two-color excitation of a hematoporphyrin derivative could be used to photodegrade *L*-tryptophan from upper triplet states as an oxygen-independent mechanism. Smith *et al.*<sup>19</sup> demonstrated that two-color excitation of Rose Bengal *in vitro* caused cell death in the absence of oxygen, presumably by toxic photoproducts produced from higher excited states. The ability to photosensitize tissues that are low in oxygen, such as hypoxic tumor regions, is of great significance in the long-term outcome for a variety of tumor treatment modalities. These hypoxic tumor regions often present resistance to photosensitization and radiosensitization and, in some cases, to chemotherapy.<sup>20</sup> Although there has recently been interest in finding appropriate radical-producing photosensitizers,<sup>21</sup> there has been little study of how to exploit short laser pulses to sensitize reactions in scattering media such as tissue. This is a complex issue, since the PDT absorbed light dose will depend on several effects, such as saturation of the ground-state absorption, excitation to upper excited singlet and triplet states, and

permanent photobleaching of the sensitizer, with each of these effects occurring at different rates at different depths.

The goal of this study was to examine the absorbed PDT dose, defined as the total number of photons absorbed by the photosensitizer per unit volume, delivered to tissue-like media for both cw- and pulsed-laser irradiation. A gelatin-based tissue-simulating dosimetry system was developed with optical scattering and absorption properties similar to tissue and containing both a photosensitizer molecule and a reporter molecule as a photochemical actinometer.<sup>22,23</sup> The reporter molecule provides a fluorescent signal when activated by the excited-state photosensitizer or other reactive molecular species that simulate tissue photosensitization. Thus, the yield of this fluorophore depends on both the integrated light fluence and the local photosensitizer absorption, both of which contribute to the PDT dose. Using these dosimeters, the depth profile of the accumulated PDT dose under different irradiation conditions could be examined in a well-controlled *in vitro* system, avoiding the biological variability inherent in animal experiments. The parameters varied in this study include the irradiance, the surface radiant exposure (sometimes referred to as dose or incident fluence), the photosensitizer concentration, and the optical absorption and scattering coefficients of the medium. Numerical simulations of the light propagation were used to confirm and interpret the experimental results.

These experiments provide (1) direct observations of the PDT dose in a tissue-simulating phantom for both cw and pulsed irradiation and (2) the background dosimetry needed to properly plan *in vivo* PDT experiments with pulsed irradiation.

## 2. Materials and Methods

### A. Dosimeter Chemistry

The reporter molecule DCF-DA (Molecular Probes Inc., Eugene, Oregon) has, in its original form, negligible absorption and fluorescence throughout most of the visible spectrum. It has been used as a probe molecule for hydrogen peroxide detection in solution<sup>24</sup> and in cell culture.<sup>25–27</sup> The oxidized form of the DCF-DA molecule has a strong absorption band (peak at 485 nm) and fluorescence (peak at 528 nm). The exact chemical structure of the oxidizing species is not known; however, DCF-DA is oxidized through a variety of reactions, including those with excited state photosensitizers.<sup>24–27</sup> In this study, the photosensitizer BPD-MA (Quadra Logic, Vancouver, Canada) was used. The excitation of BPD-MA with 690-nm light produces singlet oxygen<sup>28</sup> and various other photoproducts.<sup>29</sup>

Both DCF-DA and BPD-MA were predissolved in dimethyl sulfoxide (DMSO) as 1-mg/ml stock solutions and frozen until needed. Solutions and gelatin-based solids were made from the DMSO stock solutions by dilution with phosphate-buffered saline (PBS). The relative concentrations of both BPD-MA and oxidized DCF-DA were quantified by fluores-

cence spectroscopy. The absolute concentration of oxidized DCF-DA produced was calculated by comparison with calibrated fluorescence measurements of pure DCF (Acros Organics, New Jersey), measured in solutions with the same proportion of DMSO and PBS as in the dosimeters. Initial calibration of the fluorescence intensities in nonscattering solutions and gelatin solids was done on a standard fluorometer system (SPEX Industries, Massachusetts), with plastic cuvettes of 1-cm optical path length.

It was found that incorporating BPD-MA and DCF-DA into the PBS-based gelatin slightly decreased the yield of oxidized DCF-DA produced, when compared with the PBS solution, but did not alter the linearity of the process. The gelatin-based mixtures were very sensitive to temperature and ambient light, so they were kept in a sealed, opaque container at 5 °C before and after irradiation.

The absorption spectrum of the photosensitizer within gelatin was measured on a Hewlett-Packard spectrometer with standard 1-cm cuvettes. The absorption of BPD in gelatin was also determined at high light intensities by measurement of the transmission of 10-ns laser pulse energies at 690 nm through 1-cm quartz cuvettes of gelatin, referenced to gelatin without BPD-MA. A concentration of 7.90  $\mu\text{M}$  BPD-MA was used, and transmission energies were measured with a Laser Precision RJ-7610 radiometer.

The molecular diffusion coefficient of DCF-DA in gelatin was measured by examination, as a function of time, of the spreading of a fluorescent spot produced in a 3-mm-thick layer of gelatin. Focusing the cw laser to a 2-mm-diameter irradiation spot produced a localized circular region of oxidized DCF-DA. The fluorescent image of this spot was captured for a series of time points after the irradiation, to as long as 2 h, with a CCD camera coupled to a fluorescence microscope. The time to expand from a 2 mm to a 3 mm FWHM spot was approximately 1 h. The FWHM versus time was fitted to a diffusion equation, as described in previous studies,<sup>22</sup> to determine the molecular diffusion coefficient.

#### B. Tissue-Simulating Dosimeters

The optical characteristics of tissue can be simulated in a medium that has the appropriate elastic scattering and absorption coefficients. The tissue-simulating dosimeters were made of gelatin with 7% solids (Knox brand) dissolved in boiling PBS, titanium dioxide powder,  $\text{TiO}_2$  (Fisher Chemical, Boston, Massachusetts), and India ink. The  $\text{TiO}_2$  provides high scattering with relatively little absorption, while the India Ink provides the converse.<sup>30,31</sup> The dosimeters were mixed in 20-ml quantities, stirred for 2 min, and left to solidify at 5 °C for 24 hs. Cylindrical dosimeters 2.5 cm in diameter and 3.0 cm in length were used for the experiments. The 1–2-mm end layers of the gelatin phantoms were cut off, before irradiation, to eliminate inhomogeneities in the scattering that were due to settling and surface tension.

The optical scattering and absorption coefficients of

different types of tissue vary considerably.<sup>32</sup> For most of this study the reduced scattering coefficient at 690 nm was set at  $\mu_s' = 1.4 \pm 0.2 \text{ mm}^{-1}$  by use of 0.2 g of  $\text{TiO}_2$  in 20 ml gelatin, and the absorption coefficient  $\mu_a$  was set at  $0.010 \pm 0.001 \text{ mm}^{-1}$  by use of 0.002% India ink volume by volume. The optical properties of the initial phantoms were determined with a diffuse reflectance instrument,<sup>33,34</sup> which measured the optical reflectance as a function of radial distance at 10 locations as far as 1 cm from the source fiber. These measurements were used to calculate  $\mu_a$  and  $\mu_s'$  with an inverse algorithm that matched the measured reflectance data with Monte Carlo predicted values. This system was used to measure several individual tissue phantoms to determine the intersample reproducibility of the optical coefficients.

#### C. Irradiation and Measurements

The cw light was supplied from an argon-ion-pumped dye laser operating at 690 nm (CR-599, Coherent). The pulsed light comprised 10-ns pulses from a YAG-pumped optical parametric oscillator at 690 nm (MOPO-700, Spectra-Physics) at a repetition rate of 10 Hz. The maximum time-averaged irradiance was 300  $\text{mW}/\text{cm}^2$ , which corresponds to a peak pulse irradiance of approximately 3  $\text{MW}/\text{cm}^2$ . The cw beam was delivered through a 500- $\mu\text{m}$  fiber and then collimated, after exiting the fiber, by a plano-convex lens to produce a flat-top profile beam with a diameter of 16 mm. The pulsed laser produced a 7-mm FWHM beam, which was cropped with an aperture to 4 mm and expanded with a lens system to produce a collimated 16-mm beam spot with a radial intensity variation of less than 20%. The incident power was measured immediately before and after irradiation with a calibrated powermeter (Scientec Model 365, Colorado). The irradiation geometry is shown in Fig. 1(a).

After irradiation each dosimeter was cut along the central axis, and fluorescence measurements were made with a fluorescence microscope having a 10 $\times$  objective, which probed a 0.5-mm-diameter spot, as in Fig. 1(b). The excitation light was provided by an arc lamp coupled to the microscope and filtered to either 425- or 485-nm excitation light with a 40-nm band-pass. Part of the emission light was coupled, via a fiber bundle, to an optical multichannel analyzer (EG&G Model 1460), which was used to record the fluorescence signal. The oxidized form of DCF-DA was excited at 485 nm and fluorescence monitored at a 533-nm wavelength; BPD-MA was excited at 425 nm and monitored at 696 nm. Each fluorescence measurement had a 1-s accumulation time, and successive measurements were taken at 1-mm increments along the central axis of the phantom dosimeter. Since the microscope excitation light itself could generate oxidized DCF-DA, the probe light exposure to the dosimeter was limited to less than 5 s to limit this systematic error to less than 150 cps in the scattering dosimeter measurements. The value of 150 cps was estimated by measuring the increase in fluorescence induced from probing several single spots for 30 s, which induced an average increase in the detected signal of

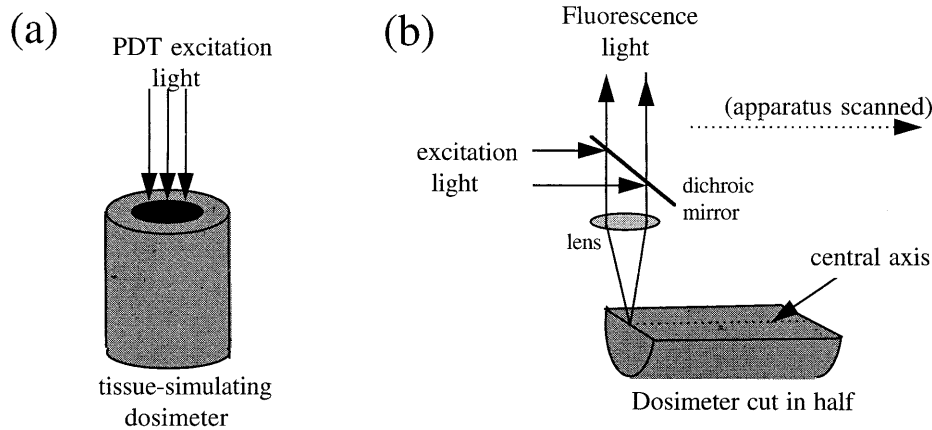


Fig. 1. (a) Geometry of the tissue-simulating dosimeter. (b) Fluorescence scanning of the dosimeter after irradiation.

45000 cps over 30 s. This variation was the limiting error for each individual phantom measurement; however, intensity fluctuations of the excitation light were thought to be the major source of error in comparing separate dosimeters. This error will be discussed further in Section 3.

#### D. Numerical Simulations

Numerical simulations of the experiment were performed to model the propagation of light in the medium with diffusion theory calculations.<sup>35-37</sup> Three-dimensional (3-D) diffusion theory was used here for both the cw and the pulsed radiation. For the cw irradiation the photon fluence rate  $\Phi(\mathbf{r}, t)$ , at any point  $\mathbf{r}$  in a scattering medium is defined as the number of photons passing through a unit spherical surface per unit time, which is given by the solution of the equation

$$-D(\mathbf{r})\nabla^2\Phi(\mathbf{r}, t) + \mu_a(\mathbf{r})\Phi(\mathbf{r}, t) = S_0(\mathbf{r}), \quad (1)$$

with the absorption coefficient,  $\mu_a = 2.303\sum\epsilon_x C_x$  ( $\epsilon_x$  is the extinction coefficient of absorber  $x$ , and  $C_x$  is the respective concentration), summed over all chemical species that absorb light at the irradiation wavelength (primarily ink and BPD-MA). The optical diffusion coefficient here is defined as  $D = (3\mu_s')^{-1}$  (when  $\mu_s' \gg \mu_a$ ), where  $\mu_s'$  is the reduced scattering coefficient, which is assumed to be constant and uniform throughout the dosimeter. The term  $S_0(\mathbf{r})$  is the source of photons per unit volume per unit time. This equation can be solved on a discrete lattice of points by a finite difference calculation,<sup>38</sup> given as

$$\begin{aligned} \Phi_{i,j,k} = [S_{0,i,j,k}/D + (\Phi_{i-1,j,k} + \Phi_{i+1,j,k} + \Phi_{i,j-1,k} + \Phi_{i,j+1,k} \\ + \Phi_{i,j,k-1} + \Phi_{i,j,k+1})/(\Delta L)^2]/[6/(\Delta L)^2 \\ + \mu_{a,i,j,k}/D], \end{aligned} \quad (2)$$

where  $\Phi_{i,j,k}$  is the discretized fluence rate at location  $(i, j, k)$  on a 3-D lattice, and  $\Delta L$  is the physical distance between points in the lattice, which was set to one mean free scattering length,  $1/\mu_s'$ . This calculation was done for all points within the specified volume and was iterated to yield the steady-state solution. The surface irradiance, dimensions, and optical properties of the

simulated volume were matched to the actual dosimeters. The absorbed light dose  $P(\mathbf{r})$  is defined here as the number of photons absorbed by the photosensitizer per unit volume of the dosimeter.  $P(\mathbf{r})$  is calculated as the time integration of the fluence rate, extinction coefficient, and photosensitizer concentration,  $C(\mathbf{r}, t)$ , during the irradiation time  $T$ ,

$$P(\mathbf{r}) = 2.303\epsilon \int_0^T \Phi(\mathbf{r}, t)C(\mathbf{r}, t)dt. \quad (3)$$

The discrete calculation of the dose  $P^n$  during time period  $\Delta t$  after  $n$  time periods is

$$P_{i,j,k}^n = 2.303\epsilon\Phi_{i,j,k}^n C_{i,j,k}^n \Delta t, \quad (4)$$

where  $C_{i,j,k}^n$  and  $\epsilon$  refer only to BPD-MA. This calculation was repeated until the irradiation period was finished, and the total number of photons absorbed per unit volume,  $P_{i,j,k}$ , was calculated by summation of  $P_{i,j,k}^n$ .

For cw irradiation the number of photons absorbed per voxel was calculated with 30-s time intervals, since the changes in photosensitizer concentration and fluence rate were slow enough. After each time step the absorption coefficient was recalculated at all spatial positions,

$$(\mu_a)_{i,j,k}^{n+1} = (\mu_a)_{i,j,k}^n - 2.303\epsilon\phi_{PB}P_{i,j,k}^n/N_A, \quad (5)$$

where  $N_A$  is Avogadro's number and  $\phi_{PB}$  is the photobleaching quantum yield. The cw fluence-rate distribution was then recalculated with Eq. 2. This process was used to simulate the dynamic changes during a cw irradiation.

Simulation of the pulsed irradiation required the calculation of  $P_{i,j,k}^n$  to be updated during the time of each laser pulse. The pulse propagation was simulated with the time-dependent diffusion equation,<sup>10,39</sup>

$$\partial\Phi(\mathbf{r}, t)/\partial t - cD\nabla^2\Phi(\mathbf{r}, t) + \mu_a(\mathbf{r}, t)c\Phi(\mathbf{r}, t) = cS_0(\mathbf{r}, t), \quad (6)$$

where  $c$  is the speed of light in the medium. This equation was discretized as

$$\begin{aligned} \Phi_{i,j,k}^{n+1} = & \Phi_{i,j,k}^n + (\Phi_{i-1,j,k}^n + \Phi_{i+1,j,k}^n + \Phi_{i,j-1,k}^n \\ & + \Phi_{i,j+1,k}^n + \Phi_{i,j,k-1}^n + \Phi_{i,j,k+1}^n - 6\Phi_{i,j,k}^n) \\ & \times (cD\Delta t)/(\Delta L)^2 - \mu_{a,i,j,k}c\Delta t\Phi_{i,j,k}^n \\ & + c\Delta tS_{0,i,j,k}^n \end{aligned} \quad (7)$$

and solved with a time step defined by  $\Delta t = 4(\Delta L)^2/(cD)$ . The number of photons from a 10-ns pulse was followed as a function of time and space as they diffused through the 3-D grid of points. During the pulse the number of photons absorbed per unit volume,  $P(\mathbf{r})$ , was calculated as in Eq. (3) at all points, for each time-step. The absorption coefficient was recalculated by subtraction of the number of molecules raised to the excited singlet state,

$$(\mu_a)_{i,j,k}^{n+1} = (\mu_a)_{i,j,k}^n - 2.303\epsilon P_{i,j,k}^n/N_A, \quad (8)$$

assuming that the excited singlet-state absorption is negligible at 690 nm. At each time step the fraction of molecules that decayed to the ground state was calculated as  $\exp(-dt/\tau)$ , where  $\tau$  is the upper singlet-state lifetime. The triplet-state production of BPD-MA in PBS is very small<sup>28</sup>; however, here in gelatin-based PBS with 1.25% DMSO there is a mixture of monomeric and aggregated species, which will result in a mixture of triplet and singlet excited states on irradiation. The precise fraction of the photosensitizer that is aggregated is not known and is difficult to determine, as is the case in tissue. After each laser pulse the molecules were assumed to return to the ground state, except for those molecules permanently bleached, so that the values of  $\mu_{a,i,j,k}$  were all reset to the original values minus the photobleached fraction. The photobleaching quantum yield was the same as for the cw case. With these calculations the absorbed dose per unit volume could be estimated as a function of both space and time for both cw and pulsed light irradiation. Similarly, the amount of photosensitizer bleaching could be calculated dynamically. A more physically accurate model of the photosensitizer molecule population changes was examined in a parallel study,<sup>40</sup> where both the singlet and the triplet states were incorporated into the model; however, there was no significant increase in the light penetration predicted from the incorporation of the triplet state. This lack of influence of the triplet lifetime is thought to be a result of the short laser pulse width (10 ns), where most of the energy passes through the dosimeter on the time scale of the singlet-state lifetime (5.2 ns), especially since the photosensitizer can be continuously repumped up to the singlet state if it decays within the time of the pulse. In general, whether the molecules are in the singlet state or the triplet state, there is a reduction in absorption from the photosensitizer that is due to the transient population change. For simplicity, the model used here included only the singlet-state lifetime.

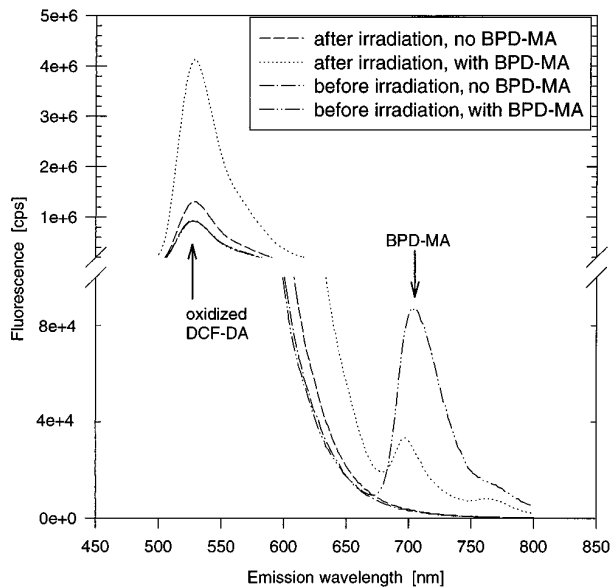
### 3. Results

#### A. Dosimetry Calibration

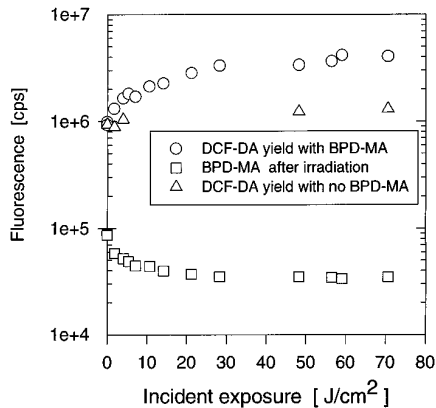
DCF-DA oxidation with excited state BPD-MA was examined by fluorimetry in non-scattering mixtures of both PBS solution and PBS-based gelatin without any TiO<sub>2</sub> or India ink. The measurements plotted in Fig. 2 were all from gelatin-filled cuvettes with 2.5 μg/ml BPD-MA and 10 μg/ml DCF-DA. Irradiation of DCF-DA in PBS at 690 nm, without photosensitizer, caused no measurable production of oxidized DCF-DA beyond that produced from ambient light. The production of oxidized DCF-DA under ambient lighting in gelatin was higher than in PBS solution, and there was also a small contribution from excitation light at 690 nm (in the absence of BPD-MA). Figure 2(a) is a plot of the fluorescence spectra from gelatin mixtures, before and after irradiation with 80 J/cm<sup>2</sup> at the BPD-MA absorption peak of 690 nm, for mixtures with and without BPD-MA. The fluorescence increase of the DCF-DA peak that is due to irradiation without BPD-MA was  $3.5 \times 10^5$  cps above background, which is an order of magnitude lower than the increase of fluorescence when BPD-MA was present, observed as  $3.3 \times 10^6$  cps above background.

In separate experiments, solutions of DCF-DA and BPD-MA were bubbled with N<sub>2</sub> and O<sub>2</sub> and irradiated at 690 nm to examine the effect of O<sub>2</sub> concentration on the DCF-DA oxidation yield. The production of oxidized DCF-DA was the same for both solutions (data not shown), suggesting that the reaction between excited-state BPD-MA and DCF-DA was not solely mediated by O<sub>2</sub>.

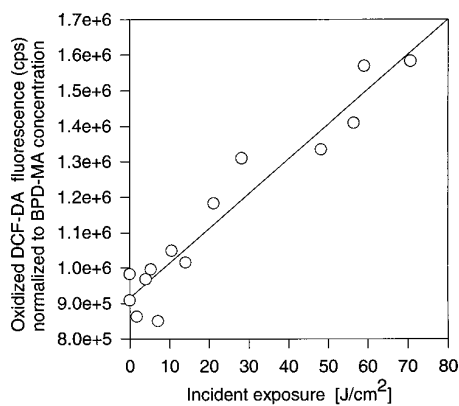
The production of DCF-DA fluorescence was linearly proportional to both the light exposure and the photosensitizer concentration, providing a stable actinometric measurement of the photoactivation of BPD-MA. As is seen in Fig. 2(b), a decrease of BPD-MA fluorescence was observed as a result of permanent photobleaching, which was mirrored by an increase in the DCF-DA fluorescence. The magnitude of the BPD-MA fluorescence was significantly lower than that of DCF-DA, since the fluorescence quantum yields for BPD-MA and DCF-DA in PBS are 0.002 and 0.90, respectively.<sup>28</sup> The fluorescence of DCF-DA was normalized to the concentration of BPD-MA by dividing the DCF-DA data by the normalized concentrations of BPD-MA at each point (the fluorescence of BPD-MA before irradiation was taken as unity). This calculation, which is plotted in Fig. 2(c), demonstrates that the production of oxidized DCF-DA is linearly proportional to the total radiant exposure. The correspondence between the bleaching of BPD-MA and the oxidization of DCF-DA suggests that the reaction responsible for oxidizing DCF-DA comes from the break-up of excited-state BPD-MA. The production of oxidized DCF-DA was found to be independent of the concentration of unoxidized DCF-DA for concentrations above 10 μg/ml, suggesting that there is an excess of DCF-DA to scavenge the excited species produced from BPD-MA. The quantum yield of oxidization for DCF-DA from



(a)



(b)



(c)

Fig. 2. (a) Fluorescence spectra of DCF-DA (10  $\mu\text{g/ml}$ ) with and without BPD-MA (2.5  $\mu\text{g/ml}$ ) in a 7% gelatin solid cuvette, for excitation at 485 nm (before and after irradiation with 80  $\text{J/cm}^2$  cw light at 690 nm). The fluorescence before irradiation was identical for both cases. (b) Measurements of fluorescence versus total incident exposure for both DCF-DA (533 nm) and BPD-MA (696 nm). Concentrations were the same as in (a). (c) Data of DCF-DA fluorescence from (b) normalized by the relative concentration of BPD-MA, as measured by the fluorescence spectrum. The solid line is a linear regression fit to the data.

excited-state BPD-MA was calculated from the change in fluorescence of the DCF-DA peak for a fixed number of BPD-MA molecules excited, calculated as

$$\Phi_{\text{DCF-DA}} = (\text{number of DCF-DA molecules oxidized}) / (\text{number of BPD-MA molecules excited})$$

$$= (\Delta F_{\text{obs}} / F_{\text{DCF}}) / (2.203 \epsilon_{\text{BPD}} C_{\text{BPD}} E A \Delta t), \quad (9)$$

where  $\Delta F_{\text{obs}}$  is the change in DCF-DA fluorescence produced by irradiation of a solution of BPD-MA at concentration  $C_{\text{BPD}}$ , using irradiance,  $E$ , in a short time period,  $\Delta t$ , and with a beam of cross-sectional area  $A$ , in a cuvette of pathlength,  $l$ . Here  $\epsilon_{\text{BPD}}$  is the extinction coefficient of BPD-MA in PBS, and  $F_{\text{DCF}}$  is the fluorescence signal per molecule of DCF measured in a series of well-calibrated solutions. Preliminary measurements indicated that fluorescence from pure DCF as compared to oxidized DCF-DA was equivalent to within 10%, indicating that their fluorescence quantum yields are almost identical. For practical purposes, the calibration measurement of  $F_{\text{DCF}}$  was done with pure DCF rather than oxidized DCF-DA to avoid the uncertainty associated with not oxidizing all of the DCF-DA molecules. The quantum yield was calculated to be  $\Phi_{\text{DCF-DA}} = 4 \times 10^{-6} \pm 0.5 \times 10^{-6}$ . This value is lower than the photobleaching quantum yield of BPD-MA,  $\Phi_{\text{PB}}(\text{BPD-MA}) = 2.8 \times 10^{-5}$ , as measured by Aveline *et al.*<sup>28</sup>

## B. Diffusion Measurement

The observed value of the molecular diffusion constant for DCF-DA in 7% gelatin solids was  $2.5 \times 10^{-5} \text{ mm}^2/\text{s}$ , as described above, measured at room temperature. These measurements indicated that the diffusion of the molecule in the gel would not result in a large redistribution of the fluorophore for the spatially-resolved measurements, within 1 h of the irradiation time. The effects of this diffusion were also minimized by refrigeration of the sample before and after irradiation and by measurement of each dosimeter within 15 min of the end of each irradiation.

## C. Dosimeter Optical Properties

The ground-state absorption coefficient of BPD-MA at 690 nm in 7% gelatin solids was measured in a spectrophotometer to be  $15200 \text{ cm}^{-1} \text{ M}^{-1}$  at 690 nm. The absorption coefficient was expected to change when a large fraction of the photosensitizer was excited; so the extinction coefficient was measured as a function of laser pulse energy fluence with 7.9  $\mu\text{M}$  BPD-MA. These measurements are plotted in Fig. 3, showing that as the laser pulse fluence increased above 10  $\text{mJ/cm}^2$  (at  $10^6 \text{ W/cm}^2$  peak irradiance) the absorption of the BPD-MA decreased from 16000  $\text{cm}^{-1} \text{ M}^{-1}$  to near 8000  $\text{cm}^{-1} \text{ M}^{-1}$ . This decrease in absorption occurred because a large fraction of the photosensitizer was excited to upper singlet and triplet states, which have lower extinction coefficients at 690 nm.

The optical calibration measurements of reduced

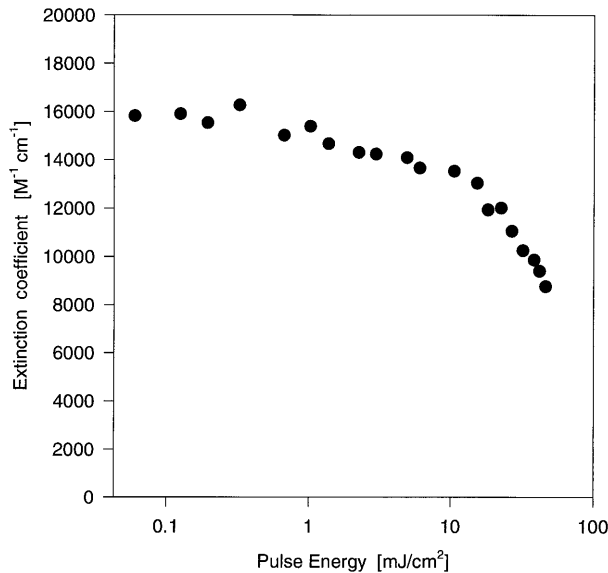
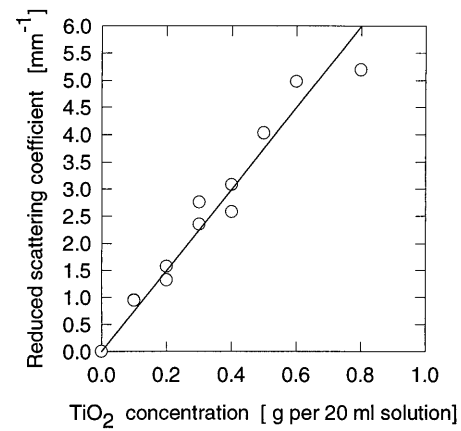


Fig. 3. Extinction coefficient versus laser-pulsed fluence with 10-ns pulses at 690 nm. Measurements of transmission through 7.9  $\mu\text{M}$  BPD-MA in 7% gelatin were used to calculate extinction relative to gelatin without photosensitizer.

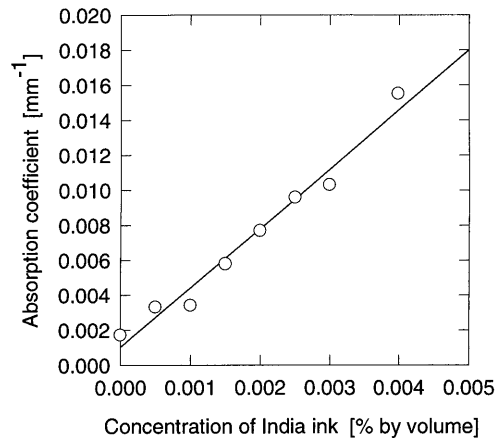
scattering coefficient versus the concentration of  $\text{TiO}_2$  in the dosimeters are plotted in Fig. 4(a). The homogeneity of the reduced scattering coefficient was better than  $\pm 10\%$  standard deviation, assessed by measurement of several parts of one sample (data not shown), and the intersample variation was also  $\pm 10\%$ . The best fit to the data shows that the scattering coefficient at 690 nm was  $\mu_s' = 7.5 \pm 0.7 \text{ mm}^{-1}$  of  $\text{TiO}_2$  in 20-ml gelatin samples for the range of concentrations shown. In Fig. 4(b) the variation of the absorption coefficient with India ink concentration is plotted for 690-nm light with a fixed  $\text{TiO}_2$  concentration of 0.30 g. The corresponding best fit for the absorption coefficient was  $\mu_a = 3.5 \pm 0.2 \text{ mm}^{-1}/\text{vol. \%}$  of India ink. For Figs. 5–8 the concentrations of  $\text{TiO}_2$  and India ink were kept fixed at 0.2 g/20 ml and at 0.002%, respectively (i.e.,  $\mu_s' = 1.5 \text{ mm}^{-1}$  and  $\mu_a = 0.007 \text{ mm}^{-1}$ ). Most of the subsequent measurements were taken with 3.44  $\mu\text{M}$  BPD-MA in the dosimeters (except for Fig. 8), which increased the absorption coefficient at 690 nm by  $0.012 \text{ mm}^{-1}$  (as measured in PBS-based gelatin with a spectrometer).

#### D. Dose Profile: Measurement and Simulation

Dosimeter results are shown in Fig. 5 for both cw and pulsed irradiation. Figure 5(a) is a plot of the DCF-DA post-irradiation fluorescence versus depth. The fluorescence decreased nearly exponentially with depth for both light conditions, except for pulsed irradiation near the surface. The control dosimeter without BPD-MA showed that the background generation of oxidized DCF-DA was a factor of 20–30 lower than with BPD-MA. Figure 5(b) shows the corresponding plots for BPD-MA fluorescence. In this case the control dosimeter included BPD-MA but



(a)



(b)

Fig. 4. (a) Measurements of reduced scattering coefficient versus  $\text{TiO}_2$  concentration for tissue-simulating dosimeters, at 690 nm, as calculated from diffuse reflectance measurements. Mixtures were 7% gelatin solids and 0.002% India ink solution in 20 ml PBS. The straight line is a linear regression fit to the data. (b) Measurements of absorption coefficient versus India ink concentration, as percent by volume. Composition as in (a) except with fixed 0.3 g of  $\text{TiO}_2$  in 20 ml. The straight line is a linear regression fit to the data.

was not irradiated, and the other data were normalized to the average BPD-MA fluorescence from this case. A decrease in BPD-MA fluorescence was observed toward the irradiated surface, owing to permanent photobleaching.

The numerical simulations incorporating light propagation, photosensitizer absorption, and photobleaching are also shown in Fig. 5. Except for an overall scaling factor, the only parameter varied to fit the experimental BPD-MA fluorescence was the photobleaching quantum yield, and a value of  $2.0 \times 10^{-5}$  gave the best fit. This value is close to the yield observed by Aveline *et al.*<sup>28</sup> of  $2.8 \times 10^{-5}$  for BPD-MA in PBS alone. However, the data in Fig. 2(b) show a biexponential decay in the fluorescence of BPD-MA, which is presumably due to interaction with the gelatin and to the molecules' existing in monomeric and aggregated forms. Aveline *et al.*<sup>28,41</sup> showed that

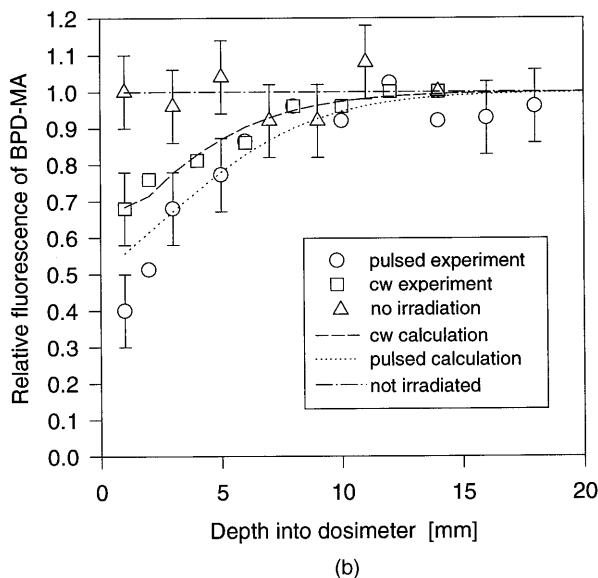
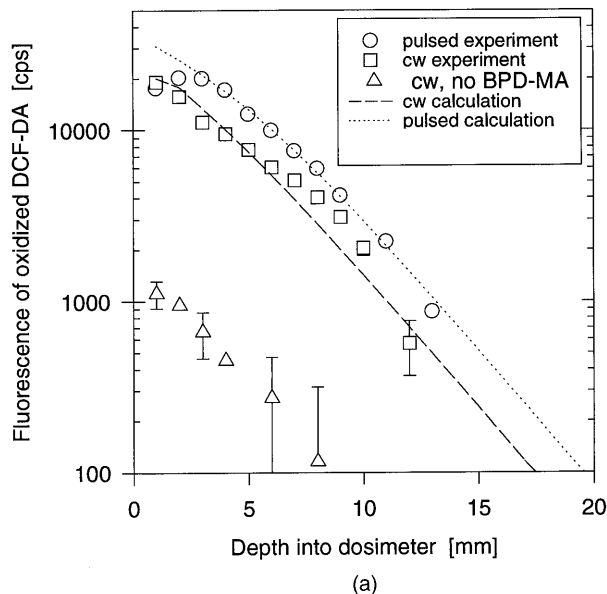


Fig. 5. (a) DCF-DA fluorescence versus depth in three dosimeters exposed to  $96 \pm 2 \text{ J/cm}^2$  at 690 nm, two with BPD-MA present and one without. Average irradiances were  $160 \text{ mW/cm}^2$  pulsed and  $110 \text{ mW/cm}^2$  cw. The lines represent simulated absorbed doses, with using the same concentration of BPD-MA ( $2.5 \text{ } \mu\text{g/ml}$ ) and optical interaction coefficients ( $\mu_s' = 1.4 \text{ mm}$  and  $\mu_a = 0.01 \text{ mm}^{-1}$ ), normalized to best fit the two data sets with a single fitting parameter. (b) BPD-MA fluorescence versus depth for the same conditions as (a). The lines are calculated values for a photobleaching quantum yield of  $2 \times 10^{-5}$ .

the photobleaching quantum yield depends on the aggregation state of the molecule as compared with monomeric forms or when molecules are bound to proteins such as human serum albumin. The calculated number of photons absorbed per unit volume was fitted to the curves of DCF-DA fluorescence for both the cw and the pulsed irradiation [shown in Fig. 5(a)] with the same scaling factor. An oxidized DCF-DA fluorescence value of 2000 cps corresponds to a calculated value of  $1 \times 10^{18}$  photons absorbed per

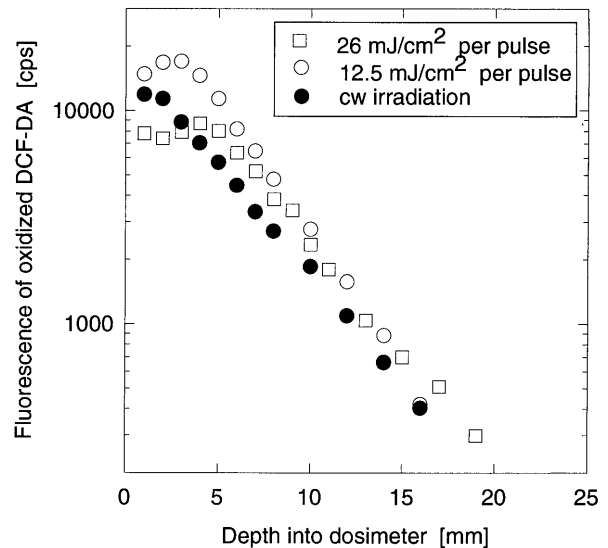


Fig. 6. Measurements of DCF-DA fluorescence for three dosimeters, irradiated at 690 nm. The peak irradiances were 1.25 and  $2.6 \text{ MW/cm}^2$  for the pulsed light and  $180 \text{ mW/cm}^2$  for the cw. The incident exposure was  $75 \text{ J/cm}^2$  in all cases.

cubic centimeter by the BPD-MA, which corresponds to a typical PDT threshold for tissue necrosis.<sup>42</sup>

Figure 6 shows the results from three dosimeters irradiated with the same radiant exposure of  $75 \text{ J/cm}^2$ , but with different irradiances. Two dosimeters were irradiated with the pulsed laser system, corresponding to pulse energies of  $12.5$  and  $26 \text{ mJ/cm}^2$  (peak powers of  $1.25$  and  $2.6 \text{ MW/cm}^2$ , respectively), and the third dosimeter was exposed to cw light at an irradiance of  $180 \text{ mW/cm}^2$ . The cw production of oxidized DCF-DA demonstrated a simple exponential behavior, as was expected from the attenuation of the light. However, the pulsed irradiations caused a deviation from the single exponential near the surface, with the higher pulse energy resulting in the lower production of DCF-DA at the surface of the dosimeter.

The dosimeters were used to examine the depth for a constant level of DCF-DA fluorescence (2000 cps) as a function of incident light exposure and BPD-MA concentration. The 2000 cps value provides an isodose level to allow us to compare the effectiveness of light penetration for different irradiation conditions and also corresponds to the approximate threshold for tissue necrosis. Figure 7 shows the results plotted versus the total radiant exposure, with each point representing a separate dosimeter. The scatter in the data is due to light intensity fluctuations of the arc lamp used for excitation in the microscope and indicate that the sample-to-sample depth measurement variation was 1 to 2 mm at most. However, by taking several sample measurements over a range of exposures, it was possible to perform linear regression on the data of Fig. 7 and to estimate the average depth for DCF-DA fluorescence of 2000 cps versus the logarithm of the optical exposure to better than 1 mm. The lines in Fig. 7 are the linear regression

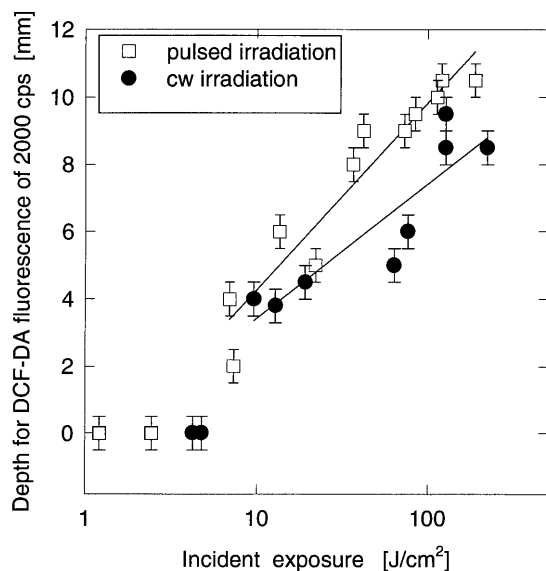


Fig. 7. Depth for fixed DCF-DA fluorescence of 2000 cps versus incident fluence. Each point represents a separate dosimeter, and the error bars represent the intensity and positioning uncertainties. The average irradiances were 110 mW/cm<sup>2</sup> for cw and 150 mW/cm<sup>2</sup> for the pulsed (i.e., 1.5 MW/cm<sup>2</sup> peak irradiance).

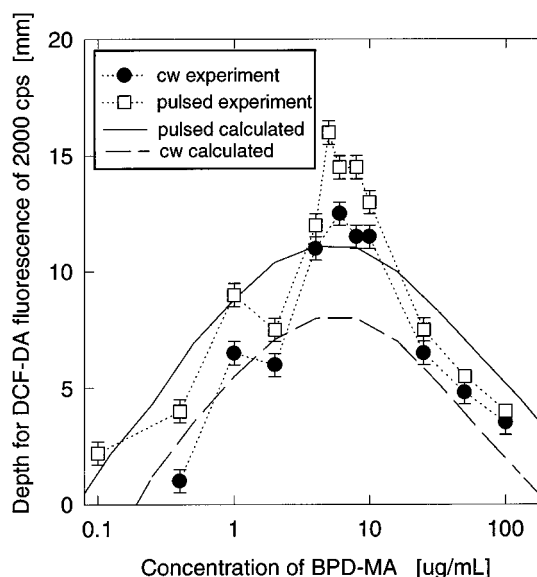


Fig. 8. Depth of penetration for DCF-DA fluorescence of 2000 cps versus concentration of BPD-MA, for DCF-DA fixed at 10 µg/ml. Irradiation was at 690 nm with 1.4 MW/cm<sup>2</sup> peak pulsed, 102 mW/cm<sup>2</sup> cw, for a total incident exposure of 84 J/cm<sup>2</sup> for both. The lines are calculated values for  $5 \times 10^{17}$  photons absorbed per cm<sup>3</sup> using the same values of  $\mu_a$  and  $\mu_s'$  as the dosimeters.

fits, excluding the points of zero depth, since there is a threshold effect at approximately 8–9 J/cm<sup>2</sup> incident exposure. The average increase in depth for 2000 cps for the pulsed data versus the continuous wave data is  $1.5 \pm 0.6$  mm/log of exposure, and the probability for this difference is  $P \cong 0.032$ , based upon the standard  $T$  test of the slopes from the linear regression.

Photosensitizer concentration in the dosimeters was varied from 0.1 to 100 µg/ml, with a fixed concentration of unoxidized DCF-DA of 1.0 mg/ml. All dosimeters were exposed to 64 J/cm<sup>2</sup> for cw and pulsed irradiation with irradiances of 110 and 150 mW/cm<sup>2</sup>, respectively. The measured depths for 2000 cps of DCF-DA fluorescence are plotted in Fig. 8. The effective treatment depth increased approximately linearly with the logarithm of photosensitizer concentration up to  $\sim 5$  µg/ml, and decreased for higher concentrations. The simulation data plotted corresponded to a best-fit value of  $5 \times 10^{17}$  photons absorbed per cm<sup>3</sup>. This calculated value of the absorbed dose was chosen as a best fit to the experimental data, rather than our using the same value as above. Although the agreement between experiment and theory was not exact, the features of the data are represented by the theoretical lines.

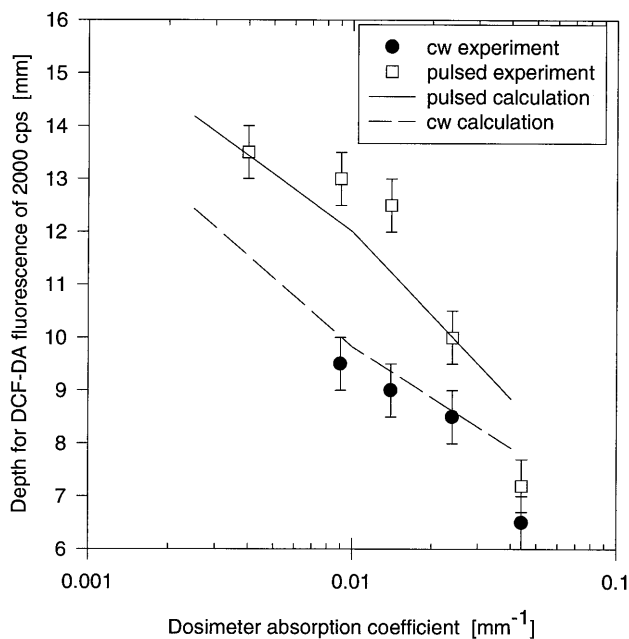
To allow us to examine the effects of varying the optical properties of the medium, dosimeters were made with fixed concentrations of BPD-MA and DCF-DA and varying concentrations of TiO<sub>2</sub> and India ink. Each dosimeter was irradiated with a total incident exposure of 84 J/cm<sup>2</sup>. The range of scattering and absorption coefficients corresponded to typical tissue values.<sup>32</sup> The experimental values are plotted in Fig. 9. The simulation results in Fig. 9

correspond to a best fit of  $5 \times 10^{17}$  photons absorbed per cubic centimeter.

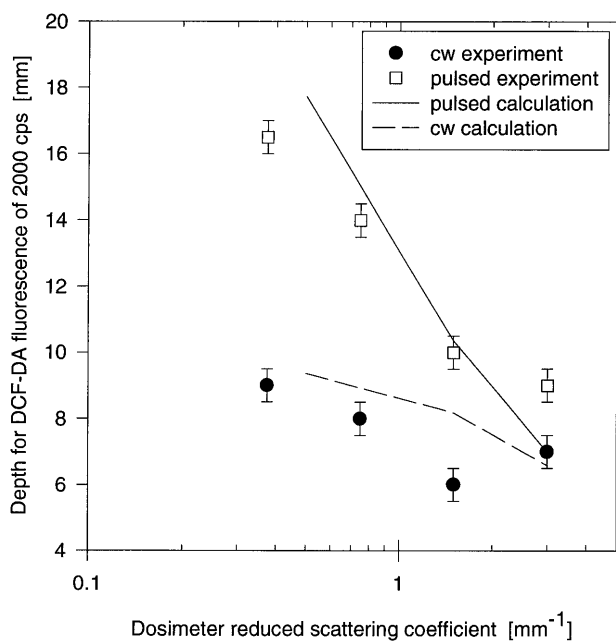
#### 4. Discussion

The PDT dose from photosensitizer absorption has been experimentally determined through the use of tissue-simulating dosimeters and has been confirmed by theoretical modeling. The results are consistent with the hypothesis that oxidized DCF-DA fluorescence is proportional to the PDT absorbed light dose and serves as a true reporter of the photodynamic effect. In all experiments the penetration of light into the dosimeters was higher for pulsed laser light than for cw light, which is consistent with transient population changes lowering the average absorption coefficient of the medium and is consistent with data of Fig. 3.

The production of oxidized DCF-DA in clear gelatin samples shown in Fig. 2 shows a linear dependence on the product of the photosensitizer concentration and the total light exposure. All the preliminary calibration measurements were consistent with the oxidization of DCF-DA resulting from interaction with excited-state BPD-MA. Since the quantum yield of the reaction was lower than the quantum yield of BPD-MA photobleaching, it is possible to hypothesize that the reaction is a result of BPD-MA intermediate photoproducts chemically reacting with the DCF-DA. If the production of DCF-DA were entirely due to the photoproducts of BPD-MA, only 14% of the permanently photobleached BPD-MA would result in production of oxidized DCF-DA. However, the exact reaction chemistry pathway is not fully understood and is difficult to examine because of the low



(a)



(b)

Fig. 9. Depth of penetration for DCF-DA fluorescence of 2000 cps versus (a) a variation in the India ink concentration and (b) a variation in the  $\text{TiO}_2$  concentration in the dosimeters. The lines are calculated for  $5 \times 10^{17}$  photons absorbed per cubic centimeter for the same  $\mu_a$  and  $\mu_s'$  values. Irradiation was at 690 nm with 1.4 MW/cm<sup>2</sup> peak pulsed and 102 mW/cm<sup>2</sup> cw, for a total incident exposure of 84 J/cm<sup>2</sup> for both cases.

quantum yield of the reaction. Despite this limitation, the DCF-DA molecule provides a robust and accurate method of recording the spatially resolved relative PDT dose in an environment that optically simulates tissue.

Since the data of absorbed dose in Fig. 5(a) follow

the predicted light fluence in the medium (lines in the same figure), these data demonstrate the linear dependence of the oxidization process with local fluence for cw irradiances. The fluence distributions in highly scattering medium are well predicted by diffusion theory modeling, and here the calculated absorbed dose varied linearly with the local light fluence. In an optically diffuse medium the fluence is attenuated exponentially with the effective attenuation coefficient,  $\mu_{\text{eff}} = (3\mu_s'\mu_a)^{1/2}$ , which is  $\mu_{\text{eff}} = 0.30 \pm 0.05 \text{ mm}^{-1}$  for these dosimeters. The measured slopes from the experiment in Fig. 5(a) have best-fit  $\mu_{\text{eff}}$  values of  $0.26 \pm 0.03$  and  $0.31 \pm 0.02$  for cw and pulsed irradiation, respectively, which are in good agreement with the predicted value (the data points between 0 and 5-mm depths were neglected in this calculation, since there was high photobleaching in this region, creating an additional nonlinearity).

The hypothesis that light penetration increases with pulsed excitation is consistent with most of the results observed in Figs. 5–9 for a range of incident irradiances and total exposures. For cw irradiation there was no significant change in DCF-DA fluorescence versus depth for irradiances from 50 to 200 mW/cm<sup>2</sup> for the same total incident exposure (data not shown). With pulsed irradiation, with average irradiances in the range of 50–300 mW/cm<sup>2</sup> for the same incident fluence, the dosimeters showed a nonlinear response in the surface regions for peak incident irradiances above 1 MW/cm<sup>2</sup> (Fig. 6). The pulse energies at which the dosimeter response becomes nonlinear agrees well with the saturation of the triplet state observed by Aveline *et al.*<sup>28</sup> and coincide with the pulse fluence at which a lowering of the extinction coefficient occurs (Fig. 3). At these high peak radiance exposures the excited states can be saturated by the 10-ns laser pulse, causing less absorption in the surface layers of the dosimeter. This saturation should cause a plateau in the DCF-DA fluorescence versus depth in the surface regions, which can be observed in Fig. 6 for the 2.6-MW/cm<sup>2</sup> peak pulse irradiance data. In the surface regions of these dosimeters, the highest concentrations of excited-state photosensitizer are produced, which could result in nonlinear processes. Another possible reason for the observed saturation at high pulse intensities could be a nonlinear response of the DCF-DA dosimeter owing to competing routes of photosensitizer decay, which results in a lower production of oxidized DCF-DA. In any case, the yield of the dosimeter was not affected at greater depths, and the profiles of DCF-DA fluorescence versus depth were consistent for the two different pulsed irradiances (Fig. 6), with cw irradiation producing significantly less oxidized DCF-DA than pulsed irradiation. The numerical simulation plotted in Fig. 5(a) does not exhibit the same level of saturation as the experimental data; however, at high simulated optical doses there is increased saturation in the upper 5 mm of the dose profile. It is likely that this discrepancy is due to a mismatch between the predicted light fluence in the phantom and the real light fluence, possibly from

uncertainties in the anticipated optical properties of the dosimeters. This discrepancy between theory and experiment is still not fully understood, yet the qualitative aspect of saturation is similar for both cases.

To quantitatively compare the PDT dose profiles for different irradiation conditions and different optical properties, a specific value of DCF-DA fluorescence was chosen to represent the effective PDT treatment depth. Several authors demonstrated a distinct threshold for the product of light exposure and photosensitizer concentration required for tissue necrosis,<sup>13,14,42–45</sup> corresponding to a lower limit of the absorbed dose by the photosensitizer necessary to generate sufficient singlet-state oxygen to kill the tissue, assuming ubiquitous oxygen supply. This threshold value depends upon many variables, such as tissue type, oxygenation, photosensitizer micro localization, and other photosensitizer properties, so there is no universal value of the threshold dose. In the case of these dosimeters, a specific level of DCF-DA fluorescence would correspond to a particular absorbed light dose, similar to a threshold value. A comparison of the measured results and computer calculations shows that the level of 2000 cps in the dosimeters corresponds to an absorbed dose,  $P(\mathbf{r})$ , of approximately  $10^{18}$  photons/cm<sup>3</sup>, which is close to the predicted threshold for tissue necrosis observed by Farrell *et al.*<sup>42</sup> for Photofrin in rat liver tissue. The variations in the depth measurement were of the order of 1–2 mm, resulting from intensity fluctuations in the arc lamp, so that multiple measurements were taken to ensure the accuracy of the results. Figure 7 shows the depth for 2000 cps measured from 24 separate dosimeters and the lines of best fit for each irradiation condition. The coefficient of linear correlation for the two lines are  $r = 0.91$  and  $r = 0.80$  for the pulsed and the cw irradiation data, respectively. The pulsed light produced greater depth penetration than the continuous irradiation on average, which is much more obvious and statistically significant in the data of Fig. 9.

At high concentration, absorption due to the photosensitizer itself can limit the observed depth of necrosis in PDT,<sup>13,14,46</sup> owing to decreased light penetration, as shown in Fig. 8. For BPD-MA concentrations below 1  $\mu\text{g/ml}$  the dominant optical properties were the intrinsic scattering and absorption coefficients of the medium, and the additional absorption resulting from the photosensitizer decreased during irradiation owing to permanent photobleaching. Above  $\sim 5 \mu\text{g/ml}$  the light fluence is significantly attenuated. It is interesting to note that typical clinical drug levels are, coincidentally, similar to the optimal concentrations of photosensitizer for light penetration and that the results here are in good agreement with *in vivo* animal data.<sup>13,14,47</sup> The concentration giving the maximum treatment depth should increase with the tissue absorption coefficient.

The final parameters examined were the intrinsic optical properties of the medium. Varying either the scattering or absorption coefficient caused similar

effects in the measured depth of penetration, as is observed from the DCF-DA fluorescence (Fig. 9). Changes in the absorption affected the penetration roughly equally for both pulsed and cw irradiation. However, lower scattering coefficients caused an increase in the light penetration of the pulsed irradiation more than for cw irradiation. The simulations were in best agreement with the measured data when the theoretical value of  $5 \times 10^{17}$  photons absorbed per cubic centimeter was used. This value differed slightly from the value used in the previous fits in Fig. 5 but gave a better fit to the experimental data. In the limit of zero scattering, the excitation of photosensitizer molecules to the triplet state would be maximized, since scattering would not limit the intensity at deeper depths and hence the transient decrease in absorption would be most effective in allowing light to penetrate through the sample. Thus lower scattering in tissues could enhance the effectiveness of the pulsed light and increase the treatment depth by a factor of 2 over cw irradiation [see Fig. 9(b)], for BPD-MA in tissues with  $\mu_s' < 0.5 \text{ mm}^{-1}$  for a peak pulse irradiance greater than 1 MW/cm<sup>2</sup>.

Typical tissue scattering and absorption coefficients were simulated in the initial dosimeters (data plotted in Figs. 5–8), where the increase in depth of penetration was determined between 1 and 2 mm for the given photosensitizer dose. It is possible that permanent photobleaching of the photosensitizer may also play a significant role in increasing the depth of necrosis; however, permanent photobleaching will occur at the same rate for both pulsed and cw irradiation for the same average irradiance. The effect observed here is distinct for pulsed irradiation and can be simulated well with a computer model mimicking the transient change in absorption that should occur in the tissue. It may be possible to optimize the PDT absorbed dose by choosing a photosensitizer that has a rapid, permanent photobleaching rate that eliminates absorption in the upper tissue layers after photosensitizing has taken place to the degree appropriate to cause tissue necrosis. This effect could be examined by measuring the photobleaching rates of different photosensitizers and comparing them to the light dose needed to cause tissue necrosis.

Dosimeters were used here to observe the light penetration in an ideal tissue simulating system, free from inhomogeneities such as blood vessels, oxygen distributions, skin layers, and skin lesions. As such, they have the advantage that they can provide fundamental information about the absorbed PDT dose. The ability to vary the parameters affecting treatment depth independently is particularly valuable. The experiments reported here are consistent with the *in vivo* necrosis depth measurements observed by Okunaka *et al.*<sup>16</sup> in mouse kidney sarcoma tissue, using hematoporphyrin derivative. They observed a threefold to fourfold increase in treated depth by using 0.55 MW/cm<sup>2</sup> peak pulse irradiance in 10.9-ns pulses compared with 100 mW/cm<sup>2</sup> cw irradiation.

The highest increase in depth for a fixed absorbed dose in our measurements was twofold (in Fig. 8, for  $\mu_s' = 0.25 \text{ mm}^{-1}$ ). On the basis of these measurements, it is difficult to explain the higher increase in depth of necrosis observed by Okunaka *et al.*,<sup>16</sup> especially considering that they were using hematoporphyrin derivative rather than a second-generation photosensitizer, which would have exhibited higher differences between pulsed and cw light owing to the larger difference in extinction between ground and excited states at the excitation wavelength. It is unlikely that other natural chromophores would have significant permanent or transient changes with high-intensity irradiation, yet it is not possible to rule out biological effects in these experiments. Transient changes in the population of hemoglobin are not expected to be significant, since the excited singlet-state lifetime is in the picosecond range.

In conclusion, in addition to demonstrating the use of this PDT dosimeter, these studies indicate that pulsed irradiation can in principle be beneficial in allowing deeper light penetration in tissue, given the proper peak pulse powers and photosensitizer. Clearly the practical utility of this observation may be limited by the modest effect and by the added complexity of pulsed irradiation sources with appropriate parameters. The dosimeter and numerical analysis presented here should be useful in investigating the more complex PDT sensitization methods available with high-intensity pulsed laser sources. Future extensions of this research will examine the excited-state spectrum of BPD-MA and other photosensitizers both in solution and in tissue slices to better explain the changes in the absorption spectra.

For this research B. Pogue and T. Hasan received funding from the U.S. Department of Defense program contract N00014-94-I-0927. B. Wilson, M. S. Patterson, and L. Lilge acknowledge support from the National Cancer Institute of Canada. We thank Franz Hillenkamp and Robert Redmond for helpful suggestions; Beatrice Aveline and Christopher Lambert for informative discussions; and Julie Northcott, Joe Hayward, and Tom Farrell for the use of the diffuse reflectance apparatus. We acknowledge the generous gift of BPD-MA from QLT Phototherapeutics Inc. (Vancouver, British Columbia, Canada) and the loan of the argon laser from Coherent Inc. (Palo Alto, California).

## References

1. T. J. Dougherty, "Yearly review: photodynamic therapy," *Photochem. Photobiol.* **58**, 895–900 (1993).
2. R. van Hillegersberg, W. J. Kort, and J. H. P. Wilson, "Current status of photodynamic therapy in oncology," *Drugs* **48**, 510–527 (1994).
3. C. J. Gomer, "Preclinical examination of first and second generation photosensitizers used in photodynamic therapy [review]," *Photochem. Photobiol.* **54**, 1093–1107 (1991).
4. B. W. Henderson and T. J. Dougherty, "How does photodynamic therapy work?" *Photochem. Photobiol.* **55**, 145–157 (1992).
5. D. Phillips, "The photochemistry of sensitizers for photodynamic therapy," *Pure Appl. Chem.* **67**, 117–126 (1995).
6. H. I. Pass, "Review: photodynamic therapy in oncology: mechanisms and clinical use," *J. Natl. Cancer Inst.* **85**, 443–456 (1993).
7. J. G. Levy, "Recent clinical results with benzoporphyrin derivative monoacid ring A," presented at Twenty-third Annual meeting of the American Society of Photobiology, Washington, D.C. (May 1995).
8. T. Hasan and J. A. Parrish, "Photodynamic therapy of cancer," in *Cancer Medicine* (Williams and Wilkins, Baltimore, Md., 1996), Chap. 50, pp. 739–751.
9. B. C. Wilson and M. S. Patterson, "The physics of photodynamic therapy," *Phys. Med. Biol.* **31**, 327 (1986).
10. A. E. Profio and D. R. Doiron, "Dose measurements in photodynamic therapy of cancer," *Lasers Surg. Med.* **7**, 1–5 (1987).
11. J. L. Boulnois, "Photophysical processes in recent medical laser developments: a review," *Lasers Med. Sci.* **1**, 47–63 (1985).
12. A. R. Morgan and D. Skalkos, "Second generation photosensitizers: where are we going and where should we be going?" in *Future Directions and Applications in Photodynamic Therapy*, SPIE Inst. Series **6**, 87–106 (1990).
13. S. G. Bown, C. J. Tralau, P. D. C. Smith, D. Akdemir, and T. J. Weiman, "Photodynamic therapy with porphyrin and phthalocyanine sensitization: quantitative studies in normal rat liver," *Br. J. Cancer* **54**, 43–52 (1986).
14. M. S. Patterson, B. C. Wilson, and R. Graff, "In vivo tests of the concept of photodynamic threshold dose in normal rat liver photosensitized by aluminum chlorosulphonated phthalocyanine," *Photochem. Photobiol.* **51**, 343–349 (1990).
15. J. A. Barltrop and J. D. Coyle, *Principles of Photochemistry* (Wiley, Toronto, 1978), Chap. 3.
16. T. Okunaka, H. Kato, C. Konaka, H. Sakai, H. Kawabe, and K. Aizawa, "A comparison between argon-dye and excimer-dye laser for photodynamic effect in transplanted mouse tumor," *Jpn. J. Cancer Res.* **83**, 226–231 (1992).
17. M. S. Patterson and B. C. Wilson, "A theoretical study of the influence of sensitizer photobleaching on depth of necrosis in photodynamic therapy," in *Free-Space Laser Communication Technologies VI*, G. Mecherle, ed., *Proc. SPIE* **2133**, 208–219 (1994).
18. A. A. Andreoni, "Two-step photoactivation of hematoporphyrin by excimer-pumped dye-laser pulses," *J. Photochem. Photobiol.* **1**, 181–193 (1987).
19. G. Smith, W. G. McGimpsey, M. C. Lynch, I. E. Kochevar, and R. W. Redmond, "An oxygen independent two-photon photosensitization mechanism," *Photochem. Photobiol.* **59**, 135–139 (1994).
20. P. Vaupel, F. Kallinowski, and P. Okunieff, "Blood flow, oxygen and nutrient supply, and metabolic microenvironment of human tumors: a review," *Cancer Res.* **49**, 6449–6465 (1989).
21. H. Stiel, K. Teuchner, A. Paul, W. Freyer, and D. Leupold, "Two-photon excitation of alkyl-substituted magnesium phthalocyanine: radical formation via higher excited states," *J. Photochem. Photobiol.* **80**, 289–298 (1994).
22. L. Lilge, T. J. Flotte, I. E. Kochevar, S. L. Jacques, and F. Hillenkamp, "Photoactivable fluorophores for the measurement of fluence in turbid media," *Photochem. Photobiol.* **58**, 37–44 (1993).
23. L. W. Mason, A. J. Welch, and M. J. C. van Gemert, "Photodynamic assay of light distributions in tissue phantoms," *Lasers Surg. Med.* **8**, 521–526 (1988).
24. A. S. Keston and R. Brandt, "The fluorometric analysis of ultramicro quantities of hydrogen peroxide," *Anal. Biochem.* **11**, 1–5 (1965).
25. J. A. Royall and H. Ischiropoulos, "Evaluation of 2'7'-dichlorofluorescein and dihydrorhodamine 123 as fluorescent

- probes for intracellular H<sub>2</sub>O<sub>2</sub> in cultured endothelial cells," Arch. Biochem. Biophys. **302**, 348–355 (1993).
26. C. P. Label, H. Ischiropoulos, and S. C. Bondy, "Evaluation of the probe 2',7'-dichlorofluorescein as an indicator of reactive oxygen species formation and oxidative stress," Chem. Res. Toxicol. **5**, 227–231 (1992).
  27. P. E. Hockberger, M. S. Ahmed, C. Lee, T. A. Skimina, W. Y. Hung, and T. Siddique, "Imaging of hydrogen peroxide in cultured cells using carboxy-dichlorofluorescein," in *Optical Diagnostics of Living Cells and Biofluids*, D. L. Farkas, R. C. Leif, A. V. Priezzhev, T. Asakuru, and B. J. Tromburg, eds., Proc. SPIE **2678**, 129–140 (1996).
  28. B. M. Aveline, T. Hasan, and R. W. Redmond, "Photophysical and photosensitizing properties of benzoporphyrin derivative monoacid ring A (BPD-MA)," Photochem. Photobiol. **59**, 328–335 (1994).
  29. R. Gilles, N. Kollias, T. Hasan, and H. Diddens, "Spectral characterization of the BPD-MA photoproduct formed in fetal calf solutions during irradiation with 690 nm cw radiation," J. Photochem. Photobiol. **33**, 87–90 (1996).
  30. M. S. Patterson, S. Anderson-Engels, and B. C. Wilson, "Absorption spectroscopy in tissue-simulating materials: a theoretical and experimental study of photon paths," Appl. Opt. **34**, 22–30 (1995).
  31. S. J. Madsen, M. S. Patterson, and B. C. Wilson, "The use of India ink as an optical absorber in tissue-simulating phantoms," Phys. Med. Biol. **37**, 985–993 (1992).
  32. W. F. Cheong, S. A. Prahl, and A. J. Welch, "A review of the optical properties of biological tissues," IEEE J. Quantum Electron. **26**, 2166–2185 (1990).
  33. B. C. Wilson, T. J. Farrell, and M. S. Patterson, "An optical fibre-based reflectance spectrometer for non-invasive investigation of photodynamic sensitizers *in vivo*," in *Future Directions and Photodynamic Therapy*, C. J. Gomer, ed., SPIE Inst. Series **6**, 219–232 (1990).
  34. T. J. Farrell, M. S. Patterson, and B. C. Wilson, "A diffusion theory model of spatially resolved, steady state reflectance for the noninvasive determination of tissue optical properties *in vivo*," Med. Phys. **19**, 879–888 (1992).
  35. A. Ishimaru, "Diffusion of a pulse in densely distributed scatterers," J. Opt. Soc. Am. **68**, 1045–1049 (1978).
  36. W. M. Star, J. P. A. Marijnissen, and M. J. C. van Gemert, "Light dosimetry in optical phantoms and in tissues. I. Multiple flux and transport theory," Phys. Med. Biol. **33**, 437–454 (1988).
  37. A. Ishimaru, "Diffusion of light in turbid media," Appl. Opt. **28**, 2210–2215 (1989).
  38. W. H. Press, S. A. Teukolsky, W. T. Vetterling, and B. P. Flannery, *Numerical Recipes in Fortran, The Art of Scientific Computing*, 2nd ed. (Cambridge U. Press, New York, 1992) Chap. 19.
  39. M. S. Patterson, B. Chance, and B. C. Wilson, "Time resolved reflectance and transmittance for the noninvasive measurement of tissue optical properties," Appl. Opt. **18**, 3484–3488 (1989).
  40. B. W. Pogue, R. W. Redmond, and T. Hasan, "Dosimetry for pulsed-laser photodynamic therapy," in *Laser-Tissue Interaction VII*, S. L. Jacques, ed., Proc. SPIE **2681**, 130–139 (1996).
  41. B. M. Aveline, T. Hasan, and R. W. Redmond, "The effects of aggregation, protein binding and cellular incorporation on the photophysical properties of benzoporphyrin derivative monoacid ring A (BPD-MA)," J. Photochem. Photobiol. B **30**, 161–169 (1995).
  42. T. J. Farrell, B. C. Wilson, M. S. Patterson, and R. Chow, "The dependence of photodynamic threshold dose on treatment parameters in normal rat liver *in vivo*," in *Optical Methods for Tumor Treatment and Early Diagnosis: Mechanisms and Techniques*, T. J. Dougherty, ed., Proc. SPIE **1426**, 146–155 (1991).
  43. M. C. Berenbaum, R. Bonnett, and P. A. Scourides, "*In vivo* biological activity of the components of haematoporphyrin derivative." Br. J. Cancer **45**, 571–581 (1982).
  44. J. C. van Gemert, M. C. Berenbaum, and G. H. M. Gijssbers, "Wavelength and light-dose dependence in tumour phototherapy with haematoporphyrin derivative," Br. J. Cancer **52**, 43–49 (1985).
  45. V. H. Fingar, W. R. Potter, and B. W. Henderson, "Drug and light dose dependence of photodynamic therapy: a study of tumor cell clonogenicity and histologic changes," Photochem. Photobiol. **45**, 643–650 (1987).
  46. B. C. Wilson, M. S. Patterson, and D. M. Burns, "Effect of photosensitizer concentration in tissue on the penetration depth of photoactivating light," Lasers Med. Sci. **1**, 235–244 (1986).
  47. C. J. Tralau, A. J. MacRobert, P. D. Coleridge-Smith, H. Barr, and S. G. Bown, "Photodynamic therapy with phthalocyanine sensitization: quantitative studies in a transplantable rat fibrosarcoma," Br. J. Cancer **55**, 389–395 (1987).